THE JOURNAL OF PHYSICAL CHEMISTRY Letters

Letter

pubs.acs.org/JPCL

Accurate Long-Time Mixed Quantum-Classical Liouville Dynamics via the Transfer Tensor Method

Alexei A. Kananenka,[†] Chang-Yu Hsieh,[‡] Jianshu Cao,[‡] and Eitan Geva*[,†]

[†]Department of Chemistry, University of Michigan, Ann Arbor, Michigan 48109, United States

[‡]Department of Chemistry, Massachusetts Institute of Technology, Cambridge, Massachusetts 02319, United States

ABSTRACT: In this Letter, we combine the recently introduced transfer tensor method with the mixed quantum-classical Liouville method. The resulting protocol provides an accurate, general, flexible and robust new route for simulating the reduced dynamics of the quantum subsystem for arbitrarily long times, starting with computationally feasible short-time mixed quantum-classical Liouville dynamical maps. The accuracy and feasibility of the methodology are demonstrated on a spin-boson benchmark model.

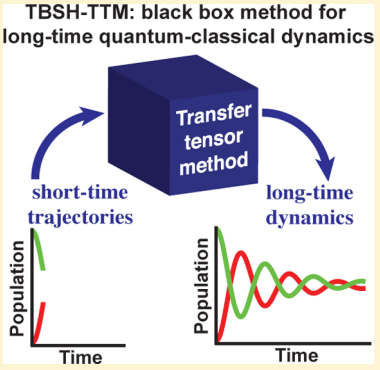

The exponential scaling of computational cost with increasing dimensionality associated with simulating quantum dynamics makes it prohibitively expensive for most systems of practical interest. Mixed quantum-classical methods, which are based on treating a small subset of degrees of freedom (DOF) quantum-mechanically while treating the remaining DOF as classical-like, therefore represent an appealing alternative when a fully quantum treatment is not possible. Several such mixed quantum-classical methods have been proposed, including ones based on a mean-field approach,[1,2] Tully's surface-hopping,[3−9] and hybrids that combine those two strategies.[10−12]

The mixed quantum-classical Liouville (MQCL) method[13−15] is arguably the most rigorous mixed quantum-classical method to date. The MQCL equation can be derived by formulating the fully quantum-mechanical dynamics within the partial Wigner representation (i.e., Wigner transforming with respect to the DOF designated as classical) and taking the limit in which the mass ratio between the classical and quantum DOF becomes small.[13,14,16−20] Alternatively, the MQCL equation can also be derived by casting the dynamics of the quantum subsystem in path integral form, and then linearizing the forward−backward action in the influence functional[21,22] with respect to the difference between forward and backward paths of the DOF designated as classical (the so-called linearized semiclassical approximation).[23,24] Furthermore, the MQCL reproduces the *exact* fully quantum-mechanical dynamics for an arbitrary quantum subsystem bilinearly coupled to a harmonic environment.

Although the computational cost involved in solving the MQCL equation is higher than that involved in either mean-field or Tully's surface-hopping techniques, it has been observed to be more accurate.[17,19,20] Several trajectory-based algorithms have been proposed over the last several years for solving the MQCL equation and approximate variations of it.[14,24−31] Two such algorithms for simulating MQCL dynamics in the adiabatic representation are the Sequential Short-Time Propagation (SSTP) algorithm[25,26] and the Trotter-Based Surface-Hopping (TBSH) algorithm.[32] Both SSTP and TBSH are based on Monte Carlo sampling of multidimensional sums, which results in a rapid increase in the number of trajectories required for convergence[33] with increasing simulation time. To reduce the number of trajectories and thereby accelerate convergence, several techniques (and their combinations) have been employed, including restricting the maximum number of nonadiabatic transitions per trajectory,[25,26,34−36] transition filtering,[32,34,36−38] and observable cutting.[25,29,35] Transition filtering amounts to rejecting nonadiabatic transitions that would otherwise lead to a rapid increase of statistical errors. Observable cutting is based on restricting the statistical weight of a trajectory if it grows beyond a certain cutoff value. The momentum-jump approximation[13,26,32] is the only approximation used in simulations of the quantum-classical dynamics with TBSH and SSTP algorithms.

While potentially useful, methods like transition filtering and observable cutting for taming the unfavorable scaling of the computational cost with increasing simulation time are based on uncontrollable approximations and often assume prior knowledge of the underlying dynamics. An alternative strategy, proposed and demonstrated by Shi and Geva,[39] is based on restricting the use of the MQCL equation to the calculation of the relatively short-lived memory kernel of the Nakajima−

Received: October 14, 2016
Accepted: November 7, 2016
Published: November 7, 2016

DOI: 10.1021/acs.jpclett.6b02389
J. Phys. Chem. Lett. 2016, 7, 4809−4814

Zwanzig Generalized Quantum Master equation (GQME).[40,41] The required theoretical framework for calculating the memory kernel from projection-free short-lived so-called system-dependent bath correlation functions, was developed by Geva and co-workers and is described in detail in refs 39 and 42. The memory kernel contains all the information required to account for the impact of the classical DOF on the quantum DOF. Importantly, the memory kernel is often observed to be short-lived with a lifetime which is significantly shorter than the relaxation time of the quantum subsystem. This implies that the memory kernel can be calculated from MQCL trajectories which are shorter than the trajectories that would be required for a direct MQCL dynamics simulation of the quantum subsystem relaxation dynamics. Once the memory kernel has been established, the GQME can be solved numerically exact for the reduced dynamics of the quantum subsystem with an arbitrarily long simulation time. More recently, Kelly and Markland have confirmed the ability of this strategy to accurately describe the long-time electronic population relaxation dynamics in the context of the spin-boson model, by calculating the memory kernel from short-time TBSH-based trajectories.[33]

In this Letter we consider the possibility of using the transfer tensor method (TTM), recently proposed by Cerrillo and Cao,[43] to extend the time range of MQCL-based simulation of the quantum subsystem reduced dynamics to arbitrarily long times, using short-time MQCL dynamical maps as input. While TTM is formally related to the above-mentioned GQME-based approach,[43] it has the advantage of being significantly easier to implement in practice. This is achieved by encoding the short-time information in terms of transfer tensors, rather than in terms of the memory kernel. As shown by Cerrillo and Cao, although the memory kernel can be obtained from the transfer tensors, this is not necessary since one can simulate the reduced quantum subsystem dynamics directly from the transfer tensors. Furthermore, obtaining the transfer tensors from short-time MQCL dynamical maps via the iterative procedure proposed by Cerrillo and Cao is straightforward, while obtaining the memory kernel via the Geva−Shi method requires calculating specialized system-dependent bath correlation functions as input and solving integral Volterra equations.[39,42] Finally, within TTM, solving for the reduced dynamics of the quantum subsystem, is accomplished via a straightforward matrix multiplication procedure, instead of by solving a set of coupled non-Markovian equations of motion. TTM has already been successfully applied to reduce the computational cost of propagating density operators with the orthogonal-polynomials-based algorithm (TEDOPA).[44] It should also be noted that TTM is wider in scope, being straightforwardly applicable to Hamiltonian classical dynamics, Brownian dynamics, and experimentally obtained time series such as single molecule spectral trajectories.

We start out by outlining the TTM protocol when applied in the context of the reduced dynamics of an open quantum system (for more details, see ref 43). The basic input for TTM consists of a set of dynamical maps $\mathcal{E}_k \equiv \mathcal{E}(t_k)$ ($t_k = k\Delta t$, $k = 0,1,2,...,k_{max}$, and Δt is the time step), defined by

$$\hat{\rho}(t_k) = \mathcal{E}_k\hat{\rho}(0) \tag{1}$$

Here, $\hat{\rho}(0)$ and $\hat{\rho}(t_k)$ are the reduced density operators that describe the state of the quantum subsystem at times 0 and t_k, respectively, and $k_{max}\Delta t$ is the memory or correlation time (defined below). In practice, k_{max} is determined by increasing its value until the quantity of interest (e.g., the time dependence of the excited state population as the system relaxes to equilibrium) becomes invariant to further increase, up to a predetermined tolerance.

It should be noted that for a quantum subsystem whose Hilbert space is of dimension N (e.g., $N = 2$ for a two-state system), $\hat{\rho}(t_k)$ can be represented by an $N \times N$ matrix, or, equivalently, by an N^2-dimensional vector in the corresponding Liouville space.[45] Thus, $\mathcal{E}_k$ is a superoperator, which can be represented by an $N^2 \times N^2$ matrix in Liouville space. TTM therefore requires dynamical maps for all possible N^4 combinations of N^2 initial and N^2 final Liouville space basis states, $\{|l\rangle\langle j|,l,j = 1,2,...,N\}$.

Assuming time translational invariance, which is consistent with the typical case of relaxation to equilibrium governed by a time-independent overall Hamiltonian, the transfer tensors, $\{T_k|k = 1,2,...,k_{max}\}$ can then be obtained iteratively from the dynamical maps, via the following identity:[43]

$$T_n = \mathcal{E}_n - \sum_{m=1}^{n-1} T_{n-m}\mathcal{E}_m \tag{2}$$

It should be noted that similarly to the dynamical maps, the transfer tensors are also represented by $N^2 \times N^2$ matrices in terms of a basis of one's choice for the quantum system Hilbert space.

Propagation of the quantum subsystem density operator can then be obtained by[43]

$$\hat{\rho}(t_{n\geq k_{max}}) = \sum_{k=1}^{k_{max}} T_k\hat{\rho}(t_{n-k}) \tag{3}$$

Here, $k_{max}\Delta t$ is the memory or correlation time, such that $T_k = 0$ for $k > k_{max}$. In practical calculations, an accuracy threshold should be defined and compared to some measure of the magnitude of the transfer tensors at every time step. The time when that measure falls below the threshold corresponds to $k_{max}\Delta t$. To obtain $\hat{\rho}(t_{n<k_{max}})$, the upper limit of the sum in eq 3 needs to be replaced by n.

Importantly, within TTM, knowledge of the dynamical maps within the finite time interval $[0,k_{max}\Delta t]$, allows one to simulate the dynamics at times longer than $k_{max}\Delta t$. Thus, even if the relaxation of the quantum subsystem occurs on a time scale longer than $k_{max}\Delta t$, it can still be calculated from dynamical input which is restricted to the time interval $[0,k_{max}\Delta t]$. It should also be noted that the transfer tensors are closely related to the memory kernel via the following identity:[43]

$$T_n = \left(1 - \frac{i}{\hbar}\mathcal{L}_s\Delta t\right)\delta_{n,1} + \mathcal{K}_n\Delta t^2 \tag{4}$$

Here, $\mathcal{K}_n = \mathcal{K}(n\Delta t)$ is the memory kernel, $\delta_{a,b}$ is the Kronecker delta and $\mathcal{L}_s(\cdot) = [\hat{H}_S, \cdot]$ ($\hat{H}_S$ is the quantum subsystem bath-free Hamiltonian). However, explicit calculation of the memory kernel is not necessary.

We next outline the MQCL method. Within this method, the state of the overall system is given in terms of an $N \times N$ matrix, where the $\alpha\alpha'$ matrix element corresponds to a time-dependent Wigner phase-space density of the classical DOF, $\rho_W^{\alpha\alpha'}(R,P,t)$ (R and P are the position and momentum of the classical DOF, assumed here to be one-dimensional for the sake of simplicity). The MQCL equation for this matrix, when cast in terms of the adiabatic representation, is given by[13,14,16−20]

DOI: 10.1021/acs.jpclett.6b02389
J. Phys. Chem. Lett. 2016, 7, 4809−4814

$$\frac{\partial}{\partial t}\rho_{\mathrm{W}}^{\alpha\alpha'}(R,P,t) = -iL_{\alpha\alpha'}\rho_{\mathrm{W}}^{\alpha\alpha'}(R,P,t) - i\omega_{\alpha\alpha'}\rho_{\mathrm{W}}^{\alpha\alpha'}(R,P,t) + \sum_{\beta\beta'}\mathcal{J}_{\alpha\alpha',\beta\beta'}\rho_{\mathrm{W}}^{\beta\beta'}(R,P,t) \tag{5}$$

The three terms on the right-hand side (RHS) of eq 5 are (in the order of appearance): (1) $iL_{\alpha\alpha'}\rho_{\mathrm{W}}^{\alpha\alpha'}(R,P,t)$, which accounts for classical propagation of the classical DOF on the potential energy surface (PES) $V_{\alpha\alpha'}(R) = (V_\alpha(R) + V_{\alpha'}(R))/2$, where $V_\alpha(R)$ is the adiabatic PES associated with adiabatic state $|\alpha;R\rangle$; (2) $i\omega_{\alpha\alpha'}\rho_{\mathrm{W}}^{\alpha\alpha'}(R,P,t)$, where $\omega_{\alpha\alpha'} = (V_\alpha(R) - V_{\alpha'}(R))/\hbar$, which gives rise to a phase factor in the case where $\alpha \neq \alpha'$, and results in dephasing upon averaging over multiple trajectories; (3) $\sum_{\beta\beta'}\mathcal{J}_{\alpha\alpha',\beta\beta'}\rho_{\mathrm{W}}^{\beta\beta'}(R,P,t)$, which accounts for nonadiabatic transitions between adiabatic states, and the associated change in momentum of the classical DOF (explicit expressions for $\{\mathcal{J}_{\alpha\alpha',\beta\beta'}\}$ can be found in ref 32.).

The elements of the dynamical map superoperator were obtained by calculating

$$\mathcal{E}_{\alpha\alpha',\beta\beta'}(t) = \int \mathrm{d}R \int \mathrm{d}P \rho_{\mathrm{W}}^{\alpha\alpha'}(R,P,t)\rho_{\mathrm{W}}^{\beta'\beta}(R,P,0) \tag{6}$$

Here, $\rho_{\mathrm{W}}^{\beta'\beta}(R,P,0)$ is the $\beta'\beta$ phase-space density at time 0 and $\rho_{\mathrm{W}}^{\alpha\alpha'}(R,P,t)$ is the $\alpha\alpha'$ phase-space density at time t. The calculation of the RHS of eq 6 is based on averaging over the specified number of trajectories generated by the TBSH method (for more details, see eq 35 in ref 32).

Within the TBSH method, one starts out by writing the propagator as a product of short time propagators (one per time step). Each of those short-time propagators is then cast as a Trotter product of the diagonal adiabatic (terms (1) and (2) above) and off-diagonal nonadiabatic (term (3) above) propagators. A momentum-jump approximation,[13,26,32] which is based on assuming that the momentum jumps associated with nonadiabatic transitions are small, then makes it possible to put the nonadiabatic propagator in a form that is consistent with a stochastic trajectory-based surface-hopping simulation algorithm (the reader is referred to ref 32 for more details). It should be noted that TBSH represents an improvement over SSTP in that TBSH requires fewer trajectories to converge and performs well in the case of strong coupling between quantum and classical DOF, where SSTP tends to become inaccurate.

Importantly, the computational cost of the TBSH method increases rapidly with increasing simulation time due to the exponential growth in the number of trajectories required for convergence. However, limiting the use of TBSH for generating short-time dynamical maps, and using those maps as input for TTM can make it possible to extend TBSH to times longer than the system correlation time, for which direct application of TBSH would be prohibitively expensive.

We now demonstrate combining TBSH-based MQCL dynamical maps with TTM to generate accurate long-time dynamics on the spin-boson model.[46] To this end, we tested TBSH-TTM on the same spin-boson examples used to demonstrate TBSH in ref 32. Owing to the form of the Hamiltonian, MQCL dynamics coincide with the exact quantum dynamics for this model. Since we use the TBSH method to solve the MQCL equation, the momentum jump approximation is the only approximation we use. Comparison to exact quantum results for the spin-boson model suggests that the momentum jump approximation is justified for the examples considered here (see below).

Following ref 32, the spin-boson Hamiltonian we used is given by

$$\hat{H} = -\hbar\Omega\hat{\sigma}_x + \sum_{j=1}^{N}\left(\frac{\hat{P}_j^2}{2M_j} + \frac{1}{2}M_j\omega_j^2\hat{R}_j^2 - c_j\hat{R}_j\hat{\sigma}_z\right) \tag{7}$$

Here, $\hat{\sigma}_z = |+\rangle\langle+| - |-\rangle\langle-|$ and $\hat{\sigma}_x = |+\rangle\langle-| + |-\rangle\langle+|$, Ω is the coupling coefficient between the two states $|+\rangle$ and $|-\rangle$, and $\{\hat{R}_j\}$ and $\{\hat{P}_j\}$ are the coordinates and momenta, respectively, of N independent harmonic bath modes of frequencies $\{\omega_j\}$ and masses $\{M_j\}$. The two-level system (TLS) operator $\hat{\sigma}_z$ is coupled linearly to the coordinates of each of the bath modes, $\{\hat{R}_j\}$, with coupling coefficients $\{c_j\}$.

The harmonic bath spectral density is given by

$$J(\omega) = \frac{\pi\hbar}{2}\zeta\omega e^{-\omega/\omega_c} \tag{8}$$

where ζ is the Kondo parameter that measures the strength of system-bath coupling and ω_c is the bath cutoff frequency.[47,48] Model parameters were adopted from refs 32, 47, 48. A more detailed discussion on simulating MQCL dynamics via the TBSH algorithm for the spin-boson model can also be found in ref 49. Dimensionless variables were used throughout, with the energy and distance units given by $\hbar\omega_c$ and $\sqrt{\hbar/M_j\omega_c}$ respectively. The initial density operator is assumed factorized $\hat{\rho}(0) = \hat{\rho}_s(0)\hat{\rho}_b$ with the initial state of the TLS given by $\hat{\rho}_s(0) = |+\rangle\langle+|$ and the initial state of the harmonic bath given by

$$\hat{\rho}_{\mathrm{b}} = Z_{\mathrm{b}}^{-1}\exp\left[-\beta\sum_{j=1}^{N}\left(\frac{\hat{P}_j^2}{2M_j} + \frac{1}{2}M_j\omega_j^2\hat{R}_j^2\right)\right] \tag{9}$$

where Z_{b} is the bath partition function and β is the reciprocal temperature.

Below, we present results for the relaxation dynamics of $\langle\sigma_z(t)\rangle$ for a TLS coupled to a bath that consist of 200 harmonic oscillators. The time step for the TBSH trajectories was set to $\Delta t = 0.05$. Approximately 10^8 trajectories were used for generating results designated as TBSH. Fewer (approximately 10^5) trajectories over the learning period, $k_{\max}\Delta t$, were used to generate the dynamical maps that serve as input for obtaining the transfer tensors leading to results designated as TTM. $k_{\max}$ in eq 3 was determined so that transfer tensors vanish at $t > k_{\max}\Delta t$.

Figure 1 shows the relaxation dynamics $\langle\sigma_z(t)\rangle$ for a TLS with $\Omega = 0.4$, weakly coupled to the bath ($\zeta = 0.09$) at low ($\beta = 12.5$) and high ($\beta = 0.25$) temperatures. Exact results were adopted from ref 50. The MQCL results, obtained by averaging over 10^8 TBSH trajectories, are observed to coincide with the exact results at short times, $t < 10$ and $t < 6$ for $\beta = 12.5$ and $\beta = 0.25$, respectively. However, the MQCL-TBSH results are also observed to become increasingly noisy at longer times, which is a reflection of the unfavorable scaling with increasing simulation time of the number of trajectories needed in order to obtain a converged result. In other words, an increasingly larger number than 10^8 trajectories is needed for convergence for simulation times longer than $t = 10$ and $t = 6$, for $\beta = 12.5$ and $\beta = 0.25$, respectively.

However, a closer examination reveals that the memory time in this case, $k_{\max}\Delta t = 2$, is significantly shorter than the TLS

DOI: 10.1021/acs.jpclett.6b02389
J. Phys. Chem. Lett. 2016, 7, 4809−4814

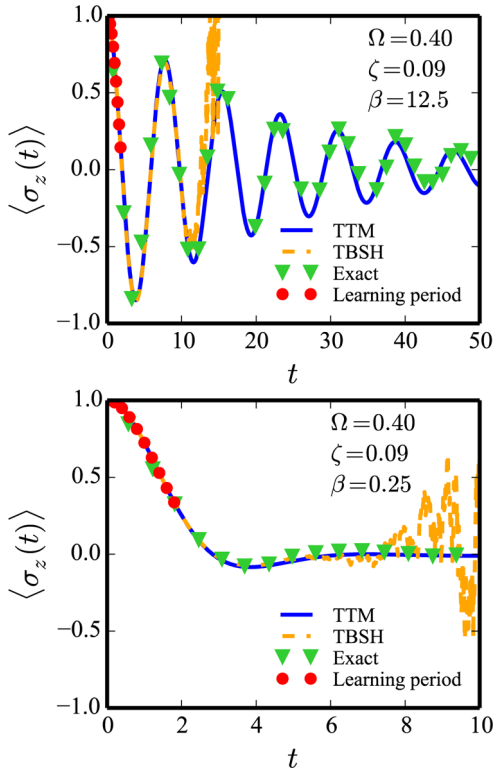

Figure 1. Relaxation dynamics $\langle\sigma_z(t)\rangle$ for a TLS with $\Omega = 0.4$, weakly coupled to the bath $\zeta = 0.09$, at $\beta = 12.5$ (upper panel), and $\beta = 0.25$ (lower panel). Shown are the exact results (green triangles), direct TBSH results (orange dashed line), and the TTM results (solid blue line) based on a learning period indicated by the red circles.

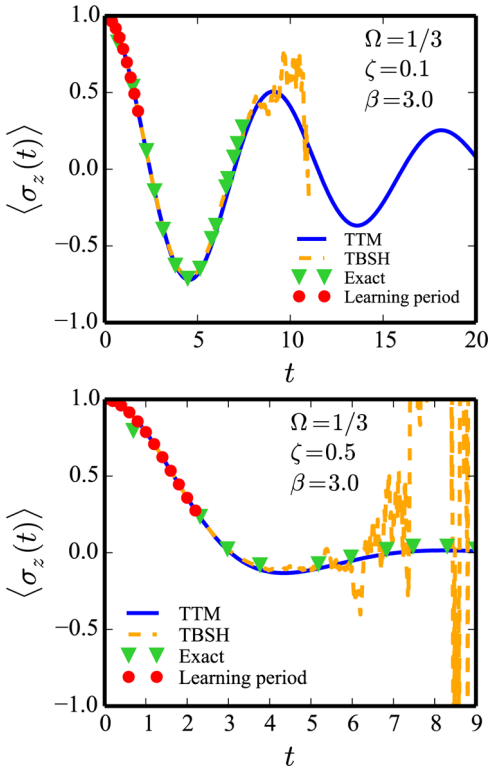

Figure 2. Relaxation dynamics $\langle\sigma_z(t)\rangle$ for a TLS with $\Omega = 1/3$, $\zeta = 0.1$ and $\beta = 3.0$ (upper panel) and $\Omega = 1/3$, $\zeta = 0.5$ and $\beta = 3.0$ (lower panel). Shown are the exact results (green triangles), direct TBSH results (orange dashed line), and the TTM results (solid blue line) based on a learning period indicated by the red circles.

relaxation time. Thus, one can generate accurate transfer tensors using dynamical maps based on as few as 10^5 trajectories of length $t = 2$ (referred to as the learning period). Using those transfer tensors within the TTM protocol, one can then simulate the TLS relaxation dynamics for arbitrarily long times. As can be seen in Figure 1, the TTM-based results essentially coincide with the exact results throughout the entire time range for which exact results are available. Thus, through TTM, MQCL dynamics of the TLS can be obtained on time scales that are significantly longer than those accessible through direct application of TBSH with a thousand times as many trajectories!

Figure 2 shows the relaxation dynamics $\langle\sigma_z(t)\rangle$ for a TLS with $\Omega = 1/3$, at $\beta = 3.0$, for two different system-bath coupling strengths, $\zeta = 0.1$ and 0.5. As for the case considered in Figure 1, results obtained via averaging over 10^8 TBSH trajectories become noisy at $t > 7$ for $\zeta = 0.1$ and $t > 5$ for $\zeta = 0.5$. However, the TTM results, obtained from dynamical maps based on only 10^5 TBSH trajectories over a learning period of $t = 2.0$ and 2.4, for $\zeta = 0.1$ and 0.5, respectively, are observed to coincide with the exact results (the latter are adopted from ref 48.). It should be noted that the increase in the learning period with increasing ζ reflects the stronger TLS-bath coupling and thereby longer lived correlations between the TLS and the bath.

Finally, in the lower panel of Figure 3 we consider the relaxation dynamics $\langle\sigma_z(t)\rangle$ for a TLS with $\Omega = 0.8$, which is strongly coupled to the bath, $\zeta = 2.0$, at $\beta = 0.25$. It should be noted that this is the only example which is somewhat different than the corresponding example in ref 32. The difference is that $\Omega = 1.2$ in ref 32 rather than 0.8 as here. The reason for the change is that $\Omega = 0.8$ provides a better example for our purposes here. The rapid TLS relaxation in this case makes it possible for the MQCL dynamics obtained via averaging over 10^8 TBSH trajectories to capture almost the entire relaxation before becoming noisy. However, here too TTM-based results with an even shorter learning period of $t \approx 1$ can reproduce the same results with far fewer (10^5) trajectories.

For comparison, the upper panel of Figure 3 shows the relaxation dynamics $\langle\sigma_z(t)\rangle$ for a TLS with $\Omega = 0.4$, which is weakly coupled to the bath, $\zeta = 0.13$, at $\beta = 1.0$. MQCL dynamics obtained via averaging over 10^8 TBSH trajectories becomes noisy at $t > 7$ for this case. However, the TTM-based result, obtained from dynamical maps based on only 10^5 TBSH trajectories over a learning period of $t = 2$ is observed to coincide with the exact results (adopted from refs 51 and 52).

In summary, in this Letter we proposed combining TTM with TBSH-based MQCL to simulate the dynamics of the quantum system for longer times than would be possible via a direct TBSH-based simulation of the MQCL dynamics. Our results clearly show that TTM makes it possible to accurately reproduce the system dynamics for arbitrarily long times by restricting the use of TBSH to calculating short-lived transfer tensors.

As with any other computational method, the accuracy of TTM relies on the accuracy of its input. Since TBSH is a stochastic method, statistical errors in the dynamical maps, and thereby in the transfer tensors, are unavoidable, and may accumulate at longer times due to the large number of transfer tensor multiplications. However, it should be noted that TTM conserves the hermiticity and trace of the system density

DOI: 10.1021/acs.jpclett.6b02389
J. Phys. Chem. Lett. 2016, 7, 4809−4814

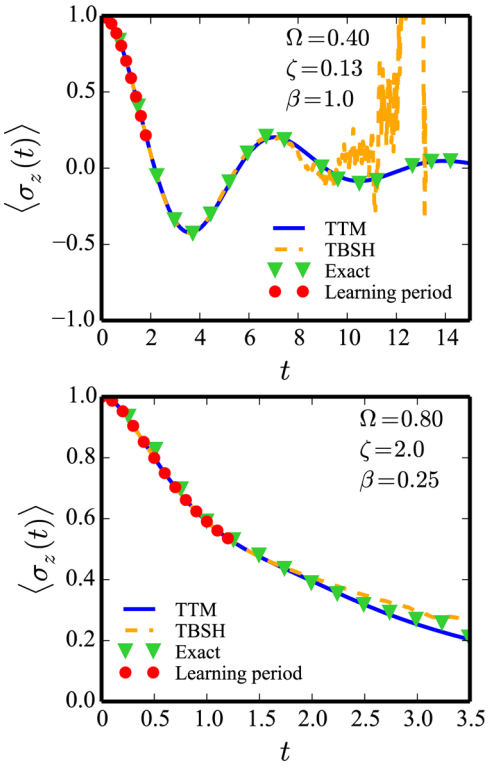

Figure 3. Relaxation dynamics $\langle\sigma_z(t)\rangle$ for a TLS with $\Omega = 0.4$, $\zeta = 0.13$ and $\beta = 1.0$ (upper panel) and $\Omega = 0.8$, $\zeta = 2.0$ and $\beta = 0.25$ (lower panel). Shown are the exact results (green triangles), direct TBSH results (orange dashed line), and the TTM results (solid blue line) based on a learning period indicated by the red circles.

operator, thereby avoiding errors that may arise from not satisfying those properties. It should also be noted that, at least for the examples shown, the agreement with the exact results clearly indicates that those errors are rather small. Furthermore, cases where the system relaxation time is much longer than the bath memory time typically correspond to the limit of weak system-bath coupling, and can therefore be treated perturbatively in terms of rate constants.

The resulting TBSH-TTM approach is expected to be particularly useful when the learning period is significantly shorter than the quantum system relaxation time. For such cases, TBSH-TTM bypasses a major obstacle that thus far limited the range of TBSH applications, namely, the rapid increase in the number of trajectories required to obtain a converged result with increasing simulation time. TBSH-TTM is expected to make applications of TBSH to realistic molecular models feasible. Work on such applications is underway in our groups and will be reported in future publications.

AUTHOR INFORMATION

Corresponding Author

*E-mail: eitan@umich.edu.

ORCID

Eitan Geva: 0000-0002-7935-4586

Notes

The authors declare no competing financial interest.

ACKNOWLEDGMENTS

J.C. would like to acknowledge support by the National Science Foundation through Grant No. CHE-1112825. E.G. would like to acknowledge support for this project by the National Science Foundation through Grant No. CHE-1464477. The computational resources and services were provided by Advanced Research Computing at the University of Michigan, Ann Arbor.

REFERENCES

(1) Gerber, R. B.; Buch, V.; Ratner, M. A. Time-dependent Self-consistent Field Approximation for Intramolecular Energy Transfer. I. Formulation and Application to Dissociation of van der Waals Molecules. *J. Chem. Phys.* **1982**, *77*, 3022−3030.

(2) Billing, G. D. Quantum Corrections to the Classical Path Theory. *J. Chem. Phys.* **1993**, *99*, 5849−5857.

(3) Tully, J. C.; Preston, R. K. Trajectory Surface Hopping Approach to Nonadiabatic Molecular Collisions: Reaction of H^+ with D_2. *J. Chem. Phys.* **1971**, *55*, 562−572.

(4) Miller, W. H.; George, T. F. Semiclassical Theory of Electronic Transitions in Low Energy Atomic and Molecular Collisions Involving Several Nuclear Degrees of Freedom. *J. Chem. Phys.* **1972**, *56*, 5637−5652.

(5) Tully, J. C. Molecular Dynamics with Electronic Transitions. *J. Chem. Phys.* **1990**, *93*, 1061−1071.

(6) Herman, M. F. A Semiclassical Surface Hopping Propagator for Nonadiabatic Problems. *J. Chem. Phys.* **1995**, *103*, 8081−8097.

(7) Coker, D. F.; Xiao, L. Methods for Molecular Dynamics with Nonadiabatic Transitions. *J. Chem. Phys.* **1995**, *102*, 496−510.

(8) Wang, L.; Akimov, A.; Prezhdo, O. V. Recent Progress in Surface Hopping: 2011−2015. *J. Phys. Chem. Lett.* **2016**, *7*, 2100−2112.

(9) Subotnik, J. E.; Jain, A.; Landry, B.; Petit, A.; Ouyang, W.; Bellonzi, N. Understanding the Surface Hopping View of Electronic Transitions and Decoherence. *Annu. Rev. Phys. Chem.* **2016**, *67*, 387−417.

(10) Kuntz, P. J. Classical Path Surface-Hopping Dynamics. I. General Theory and Illustrative Trajectories. *J. Chem. Phys.* **1991**, *95*, 141−155.

(11) Prezhdo, O. V.; Rossky, P. J. Mean-field Molecular Dynamics with Surface Hopping. *J. Chem. Phys.* **1997**, *107*, 825−834.

(12) Volobuev, Y. L.; Hack, M. D.; Topaler, M. S.; Truhlar, D. G. Continuous Surface Switching: An Improved Time-dependent Self-consistent-field Method for Nonadiabatic Dynamics. *J. Chem. Phys.* **2000**, *112*, 9716−9726.

(13) Kapral, R.; Ciccotti, G. Mixed Quantum-Classical Dynamics. *J. Chem. Phys.* **1999**, *110*, 8919−8929.

(14) Kapral, R. Progress in the Theory of Mixed Quantum-Classical Dynamics. *Annu. Rev. Phys. Chem.* **2006**, *57*, 129−157.

(15) Kapral, R. Quantum Dynamics in Open Quantum-Classical Systems. *J. Phys.: Condens. Matter* **2015**, *27*, 073201−23.

(16) Donoso, A.; Martens, C. C. Semiclassical Multistate Liouville Dynamics in the Adiabatic Representation. *J. Chem. Phys.* **2000**, *112*, 3980−3989.

(17) Santer, M.; Manthe, U.; Stock, G. Quantum-Classical Liouville Description of Multi-dimensional Nonadiabatic Molecular Dynamics. *J. Chem. Phys.* **2001**, *114*, 2001−2012.

(18) Nielsen, S.; Kapral, R.; Ciccotti, G. Mixed Quantum-Classical Surface Hopping Dynamics. *J. Chem. Phys.* **2000**, *112*, 6543−6553.

(19) Wan, C.; Schofield, J. Mixed Quantum-Classical Molecular Dynamics: Aspects of Multithreads Algorithms. *J. Chem. Phys.* **2000**, *113*, 7047−7054.

(20) Wan, C.; Schofield, J. Exact and Asymptotic Solutions of the Mixed Quantum-Classical Liouville Equation. *J. Chem. Phys.* **2000**, *112*, 4447−4459.

(21) Feynman, R. P.; Vernon, F. L., Jr. The Theory of a General Quantum System Interacting with a Linear Dissipative System. *Ann. Phys.* **1963**, *24*, 118.

(22) Makri, N.; Thompson, K. Semiclassical Influence Functionals for Quantum Systems in Anharmonic Environments. *Chem. Phys. Lett.* **1998**, *291*, 101.

DOI: 10.1021/acs.jpclett.6b02389
J. Phys. Chem. Lett. 2016, 7, 4809−4814

(23) Shi, Q.; Geva, E. A Derivation of the Mixed Quantum-Classical Liouville Equation from the Influence Functional Formalism. *J. Chem. Phys.* **2004**, *121*, 3393−3404.
(24) Bonella, S.; Ciccotti, G.; Kapral, R. Linearization Approximations and Liouville Quantum-Classical Dynamics. *Chem. Phys. Lett.* **2010**, *484*, 399−404.
(25) Hanna, G.; Kapral, R. Quantum-Classical Liouville Dynamics of Nonadiabatic Proton Transfer. *J. Chem. Phys.* **2005**, *122*, 244505.
(26) MacKernan, D.; Kapral, R.; Ciccotti, G. Sequential Short-time Propagation of Quantum-Classical Dynamics. *J. Phys.: Condens. Matter* **2002**, *14*, 9069−9076.
(27) Hanna, G.; Geva, E. Vibrational Energy Relaxation of a Hydrogen-Bonded Complex Dissolved in a Polar Liquid via the Mixed Quantum-Classical Liouville Method. *J. Phys. Chem. B* **2008**, *112*, 4048−4058.
(28) Nassimi, A.; Bonella, S.; Kapral, R. Analysis of the Quantum-Classical Liouville Equation in the Mapping Basis. *J. Chem. Phys.* **2010**, *133*, 134115.
(29) Kelly, A.; Kapral, R. Quantum-Classical Description of Environmental Effects on Electronic Dynamics at Conical Intersections. *J. Chem. Phys.* **2010**, *133*, 084502.
(30) Kelly, A.; van Zon, R.; Schofield, J.; Kapral, R. Mapping Quantum-Classical Liouville Equation: Projectors and Trajectories. *J. Chem. Phys.* **2012**, *136*, 084101.
(31) Hsieh, C.-Y.; Kapral, R. Nonadiabatic Dynamics in Open Quantum-Classical Systems: Forward-Backward Trajectory Solution. *J. Chem. Phys.* **2012**, *137*, 22A507.
(32) Mac Kernan, D.; Ciccotti, G.; Kapral, R. Trotter-Based Simulation of Quantum-Classical Dynamics. *J. Phys. Chem. B* **2008**, *112*, 424−432.
(33) Kelly, A.; Markland, T. E. Efficient and Accurate Surface Hopping for Long Time Nonadiabatic Quantum Dynamics. *J. Chem. Phys.* **2013**, *139*, 014104.
(34) Dell'Angelo, D.; Hanna, G. Self-Consistent Filtering Scheme for Efficient Calculations of Observables via the Mixed Quantum-Classical Liouville Approach. *J. Chem. Theory Comput.* **2016**, *12*, 477−485.
(35) Bonella, S.; Coker, D.; Mac Kernan, D.; Kapral, R.; Ciccotti, G. In *Energy Transfer Dynamics in Biomaterial Systems*; Burghardt, I., May, V., Micha, D., Bittner, E., Eds.; Springer Series in Chemical Physics; Springer: Berlin Heidelberg, 2009.
(36) Uken, D. A.; Sergi, A.; Petruccione, F. Filtering Schemes in the Quantum-Classical Liouville Approach to Nonadiabatic Dynamics. *Phys. Rev. E* **2013**, *88*, 033301.
(37) Sergi, A.; Petruccione, F. Sampling of Quantum Dynamics at Long Time. *Phys. Rev. E* **2010**, *81*, 032101.
(38) Uken, D. A.; Sergi, A.; Petruccione, F. Stochastic Simulation of Nonadiabatic Dynamics at Long Time. *Phys. Scr.* **2011**, *T143*, 014024.
(39) Shi, Q.; Geva, E. A New Approach to Calculating the Memory Kernel of the Generalized Quantum Master Equation for an Arbitrary System-Bath Coupling. *J. Chem. Phys.* **2003**, *119*, 12063−12076.
(40) Nakajima, S. On the Quantum Theory of Transport Phenomena. *Prog. Theor. Phys.* **1958**, *20*, 948.
(41) Zwanzig, R. Ensemble Method in the Theory of Irreversibility. *J. Chem. Phys.* **1960**, *33*, 1338.
(42) Zhang, M.-L.; Ka, B. J.; Geva, E. Nonequilibrium Quantum Dynamics in the Condensed Phase via the Generalized Quantum Master Equation. *J. Chem. Phys.* **2006**, *125*, 044106.
(43) Cerrillo, J.; Cao, J. Non-Markovian Dynamical Maps: Numerical Processing of Open Quantum Trajectories. *Phys. Rev. Lett.* **2014**, *112*, 110401.
(44) Rosenbach, R.; Cerrillo, J.; Huelga, S. F.; Cao, J.; Plenio, M. B. Efficient Simulation of non-Markovian System-Environment Interaction. *New J. Phys.* **2016**, *18*, 023035.
(45) Mukamel, S. *Principles of Nonlinear Optical Spectroscopy*; Oxford: New York, 1995.
(46) Leggett, A. J.; Chakravarty, S.; Dorsey, A. T.; Fisher, M. P. A.; Garg, A.; Zwerger, W. Dynamics of the Dissipative Two-state System. *Rev. Mod. Phys.* **1987**, *59*, 1−85.
(47) Makri, N. The Linear Response Approximation and Its Lowest Order Corrections: an Influence Function Approach. *J. Phys. Chem. B* **1999**, *103*, 2823.
(48) Thompson, K.; Makri, N. Influence Functionals with Semiclassical Propagators in Combined Forward-Backward Time. *J. Chem. Phys.* **1999**, *110*, 1343.
(49) Mac Kernan, D.; Ciccotti, G.; Kapral, R. Surface Hopping Dynamics in a Spin Boson System. *J. Chem. Phys.* **2002**, *116*, 2346−2353.
(50) Makarov, D. E.; Makri, N. Path Integrals for Dissipative Systems by Tensor Multiplication. Condensed Phase Quantum Dynamics for Arbitrary Long Time. *Chem. Phys. Lett.* **1994**, *221*, 482.
(51) Golosov, A. A.; Reichman, D. R. Classical Mapping Approaches for Nonadiabatic Dynamics: Short Time Analysis. *J. Chem. Phys.* **2001**, *114*, 1065−1074.
(52) Egger, R.; Mak, C. H. Low-temperature Dynamical Simulation of Spin-Boson Systems. *Phys. Rev. B: Condens. Matter Mater. Phys.* **1994**, *50*, 15210−15220.

DOI: 10.1021/acs.jpclett.6b02389
J. Phys. Chem. Lett. 2016, 7, 4809−4814